



**HAL**  
open science

## Evolutionary divergence of locomotion in two related vertebrate species

Gokul Rajan, Julie Lafaye, Martin Carbo-Tano, Karine Durooure, Giulia Faini, Dimitrii Tanese, Thomas Panier, Raphaël Candelier, Joerg Henninger, Ralf Britz, et al.

► **To cite this version:**

Gokul Rajan, Julie Lafaye, Martin Carbo-Tano, Karine Durooure, Giulia Faini, et al.. Evolutionary divergence of locomotion in two related vertebrate species. *Cell Reports*, 2022, 38 (13), pp.110585. 10.1016/j.celrep.2022.110585 . hal-03142570v1

**HAL Id: hal-03142570**

**<https://hal.sorbonne-universite.fr/hal-03142570v1>**

Submitted on 16 Feb 2021 (v1), last revised 9 Dec 2022 (v2)

**HAL** is a multi-disciplinary open access archive for the deposit and dissemination of scientific research documents, whether they are published or not. The documents may come from teaching and research institutions in France or abroad, or from public or private research centers.

L'archive ouverte pluridisciplinaire **HAL**, est destinée au dépôt et à la diffusion de documents scientifiques de niveau recherche, publiés ou non, émanant des établissements d'enseignement et de recherche français ou étrangers, des laboratoires publics ou privés.



Distributed under a Creative Commons Attribution 4.0 International License

1 **Evolutionary divergence of locomotion in two related vertebrate species**

2 Gokul Rajan<sup>1,2</sup>, Julie Lafaye<sup>3</sup>, Martin Carbo-Tano<sup>4</sup>, Karine Duroure<sup>1,2</sup>, Giulia Faini<sup>1</sup>, Dimitrii  
3 Tanese<sup>1</sup>, Thomas Panier<sup>3</sup>, Raphaël Candelier<sup>3</sup>, Jörg Henninger<sup>5</sup>, Ralf Britz<sup>6</sup>, Benjamin  
4 Judkewitz<sup>5</sup>, Christoph Gebhardt<sup>2,7</sup>, Valentina Emiliani<sup>1</sup>, Georges Debregeas<sup>3</sup>, Claire Wyart<sup>4</sup>,  
5 Filippo Del Bene<sup>1,2\*</sup>

6

7 <sup>1</sup>Sorbonne Université, INSERM, CNRS, Institut de la Vision, F-75012 Paris, France

8 <sup>2</sup>Institut Curie, PSL Research University, INSERM U934, CNRS UMR3215, Paris, France

9 <sup>3</sup>Sorbonne Université, CNRS, Institut de Biologie Paris-Seine (IBPS), Laboratoire Jean Perrin  
10 (LJP), 75005, Paris, France

11 <sup>4</sup>Institut du Cerveau (ICM), Sorbonne Universités, UPMC Univ Paris 06 CNRS UMR 7225,  
12 Inserm U1127, Hôpital Pitié-Salpêtrière, 75013 Paris, France

13 <sup>5</sup>Charité–Universitätsmedizin Berlin, Einstein Center for Neurosciences, NeuroCure Cluster of  
14 Excellence, Berlin, Germany

15 <sup>6</sup>Senckenberg Naturhistorische Sammlungen Dresden, Museum für Zoologie, Dresden,  
16 Germany

17 <sup>7</sup>present address: Mortimer B. Zuckerman Mind Brain Behavior Institute, Columbia University,  
18 New York, NY, USA

19

20 **Key words:** *Danionella translucida*; *Danio rerio*; evolution; locomotion; neuronal circuits

21

22 \*Corresponding author: [filippo.del-bene@inserm.fr](mailto:filippo.del-bene@inserm.fr)

23

24

## 25 **Abstract**

26 Locomotion exists in diverse forms in nature and is adapted to the environmental constraints of  
27 each species<sup>1</sup>. However, little is known about how closely related species with similar neuronal  
28 circuitry can evolve different navigational strategies to explore their environments. We  
29 established a powerful approach in comparative neuroethology to investigate evolution of  
30 neuronal circuits in vertebrates by comparing divergent swimming pattern of two closely  
31 related larval fish species, *Danionella translucida* (DT) and *Danio rerio* or zebrafish (ZF)<sup>2,3</sup>.  
32 During swimming, we demonstrate that DT utilizes lower half tail-beat frequency and  
33 amplitude to generate a slower and continuous swimming pattern when compared to the burst-  
34 and-glide swimming pattern in ZF. We found a high degree of conservation in the brain  
35 anatomy between the two species. However, we revealed that the activity of a higher motor  
36 region, referred here as the Mesencephalic Locomotion Maintenance Neurons (MLMN)  
37 correlates with the duration of swim events and differs strikingly between DT and ZF. Using  
38 holographic stimulation, we show that the activation of the MLMN is sufficient to increase the  
39 frequency and duration of swim events in ZF. Moreover, we propose two characteristics,  
40 availability of dissolved oxygen and timing of swim bladder inflation, which drive the observed  
41 differences in the swim pattern. Our findings uncover the neuronal circuit substrate underlying  
42 the evolutionary divergence of navigational strategies and how they are adapted to their  
43 respective environmental constraints.

44

## 45 **Main Text**

46 *Danionella translucida* (DT) are minute cyprinid fish that show an extreme case of organism-  
47 wide progenesis or developmental truncation which leads to a small adult body size combined  
48 with a partially developed cranium without a skull roof. This feature together with its

49 transparency throughout the adult stages makes them interesting for functional neuroscience  
50 studies allowing the imaging of the entire brain at cellular resolution<sup>3,4</sup>. However, studies on  
51 ossification in *Danionella sp.* demonstrate that most bones affected by truncation are formed  
52 later in the development of ZF<sup>5,6</sup>. Hence, in the early stages of their development, DT and ZF  
53 are highly comparable. DT and ZF are also found in similar freshwater environments in Asia  
54 and are evolutionarily very closely related<sup>2,7</sup>. This proximity is an advantage for comparative  
55 studies of larval DT and ZF as it provides a unique opportunity to understand how differences  
56 in behaviors can arise from relatively conserved neuronal circuits.

57 During undulatory swimming, animal experiences viscous and inertial forces in the fluid. Based  
58 on the body length, the hydrodynamics dictating the swimming also changes<sup>8,9</sup>. However, the  
59 body length of ZF and DT falls in a similar range of few millimeters which leads to a transitional  
60 flow regime for both (Fig. 1a-b; size range: 4.1 to 4.9 mm)<sup>8</sup>. To compare the kinematics of their  
61 spontaneous swimming, we recorded their movement with a high-speed imaging system. Larval  
62 ZF are known to swim in a beat-and-glide pattern wherein a burst of tail activity lasting ~140  
63 ms enables them to swim at high speed and is followed by a passive glide phase<sup>10</sup>. In contrast,  
64 larval DT move at low speed by continuously beating their tail for few tens or even hundreds  
65 of seconds (Fig. 1c-d, Extended Data Movies 1 and 2). To compare the fine swimming  
66 kinematics of DT and ZF, we defined kinematic parameters based on half-tail beats, a unit  
67 common to the swimming pattern of the two species. (Extended Data Fig. 1). The continuous  
68 slow swims of larval DT occur with a smaller half tail beat frequency and a smaller maximum  
69 tail angle compared to larval ZF (Fig. 1e). In head-embedded preparation, continuous and  
70 intermittent swimming patterns were observed as well in larval DT and ZF, respectively (Fig.  
71 1f): DT swims for 98.5 % of the total recording time compared to only 2% in ZF (Fig. 1g).

72 In order to test the ability of larval DT to achieve fast speeds following sensory stimulation, we  
73 examined their escape response using tap-induced escape assay (Extended Data Movie 3). Fig.

74 1h shows the striking similarity in the escape response between DT and ZF. Both fish species  
75 initiate a fast C-bend followed by a counter bend. DT was found to swim with a lower mean  
76 speed and cover a smaller distance during this period compared to ZF (Fig. 1i, Extended Data  
77 Fig. 2). On the other hand, the delay to achieve maximum speed during escape was surprisingly  
78 smaller in DT. This faster response may compensate for the relatively lower speed of DT during  
79 an escape response (Fig. 1i). Our data shows that DT are capable of executing fast swims to  
80 escape, but have evolved a slow and continuous swimming mode during spontaneous  
81 exploratory behavior.

82 We further investigated how the distinct modes of spontaneous navigation shown by both  
83 species may impact their long-term exploratory kinematics. We monitored the swim trajectories  
84 of DT and ZF in a 35 mm diameter Petri dishes as shown in Fig. 2a-b. We then computed the  
85 mean square displacement (MSD) that quantifies the area explored by the animal over a given  
86 period of time (Fig. 2c). Surprisingly, although the DT mean forward velocity is significantly  
87 lower than ZF, the MSDs are comparable. This can be understood by considering differences  
88 in heading persistence in both species. At short-time scale, the larvae tend to swim in straight  
89 lines such that their trajectories can be considered ballistic. On longer time scales, reorientation  
90 events cumulatively randomize the heading direction and the dynamics becomes diffusive-like.  
91 The ballistic-to-diffusive transition time can be estimated by computing the decorrelation in  
92 heading direction, as shown in Fig. 2d. These graphs reveal a faster randomization of heading  
93 direction in ZF compared to DT. In ZF, the decorrelation function  $R(t)$  drops down to 0.3 in ~1  
94 second, i.e. the typical inter-bout interval, then decays to 0 in 6-7 seconds. In DT,  $R(t)$  shows a  
95 small initial drop (down to 0.8) then slowly decays to 0 over the next ~8 seconds. The small  
96 initial decay in the first ~0.5 seconds can be interpreted as reflecting the short time-scale  
97 fluctuations in heading direction during run periods. The further slow decorrelation in turn  
98 results from the successive reorientation events that separate the periods of straight swimming,

99 a process reminiscent of the classical run-and-tumble mechanism of motile bacteria<sup>11,12</sup>. The  
100 time-scale of this slow decay is expected to be controlled by the interval between successive  
101 reorientation events, which is of order of 5-10 seconds.

102 To quantitatively assess the relative contribution of the ballistic vs diffusive components of the  
103 MSD over time, we estimated the former as:

104 
$$MSD_{bal}(t) = \left\langle \left[ \int_{t_0}^{t_0+t} v * R(t' - t_0). dt' \right]^2 \right\rangle_{t_0}$$

105 where  $v$  is the mean instantaneous velocity. As expected, for a purely ballistic process,  $R=1$  and  
106  $MSD_{bal} = (vt)^2$ , whereas for a purely diffusive process,  $R=0$  and  $MSD_{bal} = 0$ . For DT, this  
107 quantity correctly captures the MSD up to ~6 seconds (Fig. 2c), indicating that the ballistic  
108 component is dominant over this long initial period. In contrast, for ZF, the MSD departs from  
109 the ballistic component from 1 second onwards, i.e. after 1-2 bouts. In summary, our analysis  
110 shows that the pattern of navigation adopted by DT yields longer heading persistence, which  
111 almost exactly compensates for its intrinsically lower swimming speed and results in  
112 comparable long-term spatial explorations.

113 We next asked what selective environmental and physiological pressures might have led to the  
114 differing swimming patterns. At the environmental level, we explored the role of dissolved  
115 oxygen on these differences. During our field study in Myanmar, we found that adult DT were  
116 most abundant at the lower water levels of a small stream at ~50 cm, characterized by lower  
117 oxygen levels compared to the surface ( $O_2= 8.75$  mg/L at the surface;  $O_2= 3.5$  mg/L at 50 cm;  
118  $O_2= 2.8$  mg/L at 80 cm) (Extended Data Fig. 3a). In contrast, adult ZF are reported in waters  
119 with variable DO concentration with a median of  $5.55 \pm 1.64$  mg/L but this lacks information  
120 on the depth at which it was recorded<sup>13</sup>. In the laboratory, we tested the occupancy of larval DT  
121 and ZF in a tall water column of 36 cm height. Larval DT were found to occupy the lower zone  
122 of the water column whereas larval ZF were found in the upper zone of the water column (Fig.

123 2e). This is consistent with previous observations that ZF adults spawn in very shallow  
124 environments while adult DT spawn in the narrow spaces in the bottom of the river bed<sup>7,3</sup>. As  
125 we have seen, upper layers of a water column in the wild are richer in dissolved oxygen (DO)  
126 when compared to the bottom layers<sup>14,15</sup>. Hence, the apparent preference of DT for deeper water  
127 would accompany a lower availability of DO in the wild. This lower DO availability would  
128 have consequences on swimming at two levels: during locomotion and at rest. During  
129 locomotion, a lower DO would act as a constraint to the maximum swimming speed that can  
130 be achieved by an animal (Extended Data Fig. 3b)<sup>16</sup>. At rest, it has been shown both,  
131 experimentally and analytically, that increased body movements with reduced stationary  
132 periods would be beneficial for larval fish in a low DO environment to be able to replenish DO  
133 in its immediate surrounding. (Extended Data Fig. 2c)<sup>17,18</sup>.

134 At the physiological level, we propose that a difference in the timing of swim bladder inflation  
135 in DT and ZF might have an important role in the differences that we observed in the swimming  
136 pattern. Consistent with previous reports, we observed inflation of swim bladder in ZF by ~4-  
137 5 dpf, whereas in DT population this occurred later between 10 and 15 dpf (Fig. 2f). As has  
138 been shown previously, without a swim bladder to regulate its buoyancy, a fish might need to  
139 continuously swim and exert a downward force to actively maintain its position in the water  
140 column<sup>19</sup>. This would also promote a continuous movement as observed in DT. However, it is  
141 important to note that the delayed inflation of swim bladder alone cannot explain the difference  
142 in swimming pattern. Indeed, we evaluated swimming in a population of DT and ZF larvae at  
143 15 dpf, all with inflated swim bladders. Although a decrease was seen in the proportion of time  
144 spent swimming in 15 dpf DT when compared to 6 dpf DT, this value remained very high  
145 compared to ZF at 6 and 15 dpf (Extended Data Fig. 3d). Altogether, our data show that the  
146 slow and continuous swimming pattern of DT might be a result of a combination of factors  
147 including lower availability of DO and delayed inflation of swim bladder.

148 To determine the cellular underpinnings of the difference in swimming modes (continuous  
149 versus discrete) in the two species, we first investigated the organization of neuronal  
150 populations in DT. We initially examined reticulospinal neurons in the brainstem as these  
151 neurons projecting from hindbrain to spinal cord are known to play a role in locomotion control  
152 in all vertebrates<sup>20,21,22</sup>. We identified numerous cells of the mesencephalic nucleus of the  
153 medial longitudinal fascicle (nucMLF/nMLF), the rhombocephalic reticular formation (nucRE)  
154 and the rhombocephalic vestibular nucleus (nucVE) whose location of soma and morphology  
155 showed a high homology with cells previously described in ZF (Fig. 3b)<sup>23,24</sup>. For instance, we  
156 observed dendrites crossing the midline from the MeM cells (of nMLF) in DT as previously  
157 described in ZF (Fig. 3c). Next, we investigated the distribution of excitatory (glutamatergic)  
158 and inhibitory (glycinergic and GABAergic) neurons in the hindbrain. In ZF, these populations  
159 are described to be spatially organized in distinct stripes ordered according to their  
160 developmental age and neurotransmitter identity<sup>25,26,27</sup>. Consistent with this arrangement, the  
161 distribution of excitatory and inhibitory neurons in DT hindbrain also forms rostro-caudally  
162 running stripes (Fig. 3d-f, and cross-section in Extended Data Fig. 4). The nearly identical  
163 location of reticulospinal neurons, and the similar distribution of neuronal population points to  
164 a closely conserved bauplan of the hindbrain locomotor control region. However, homologous  
165 neurons could have different functions, as shown for neurons involved in feeding behaviors in  
166 nematodes<sup>28</sup>.

167 In order to identify functional differences in neuronal activation during spontaneous  
168 locomotion, we investigated the recruitment of neurons throughout the brain using whole-brain  
169 calcium imaging in larval DT and ZF. We generated a novel transgenic line *Tg(elavl3:H2B-*  
170 *GCaMP6s)* in DT where the calcium indicator, GCaMP6s was nuclear-targeted and expressed  
171 under a pan-neuronal promoter as previously done in ZF (Extended Data Fig. 5a-b)<sup>29</sup>. Using  
172 light sheet microscopy, we acquired a brain stack of ~200  $\mu\text{m}$  depth at ~1 volume per second



173 while simultaneously recording the tail motion in a head-embedded preparation (Extended Data  
174 Fig. 5c-d). In order to identify the supraspinal neurons recruited during spontaneous locomotion  
175 in the two species, we performed a regression analysis on the fluorescence signal of single  
176 neurons using regressors representing swimming and termination of swimming (Extended Data  
177 Fig. 5e).

178 This approach revealed neurons in the hindbrain of DT reliably recruited during the termination  
179 of swimming and that may therefore be referred as putative “stop neurons” (Fig. 4 a-b). Such  
180 stop neurons responsible for termination of locomotion have been reported in other vertebrates  
181 such as tadpole, lamprey and mice<sup>30,21,22</sup>. While the short swim events of ZF make it difficult  
182 to survey such functional cell types, DT’s long swim events offered a unique opportunity to  
183 resolve neurons active at the termination of swimming, and pinpoint motor areas recruited for  
184 movement termination. This demonstrates the benefit of employing related animal species in  
185 functional studies in addition to their obvious use in understanding evolution of neuronal  
186 circuits.

187 With respect to initiation and maintenance of swimming activity, we identified putative  
188 locomotor regions in the brain of larval DT and ZF that were highly correlated with the swim  
189 events (Fig. 4c-d, Extended Data Fig. 5). The neuronal activity in these nuclei correlated with  
190 the duration of swim events in DT and ZF (Fig. 4e), suggesting a role in the start and / or  
191 maintenance of swimming. Among these regions, we identified a strongly correlated midbrain  
192 nucleus referred to here as the Mesencephalic Locomotion Maintenance Neurons (MLMN).  
193 We decided to focus on this region as the most interesting candidate to sustain the long swim  
194 events in DT as previous work in ZF has revealed an anatomically corresponding region  
195 suggested to comprise of nMLF as well as other glutamatergic neurons which are implicated in  
196 swimming activity<sup>31,32,33</sup>. The nMLF specifically is known to have projections to the caudal  
197 hindbrain and spinal cord and plays an important role in locomotor control<sup>31,34</sup>. To dissect the

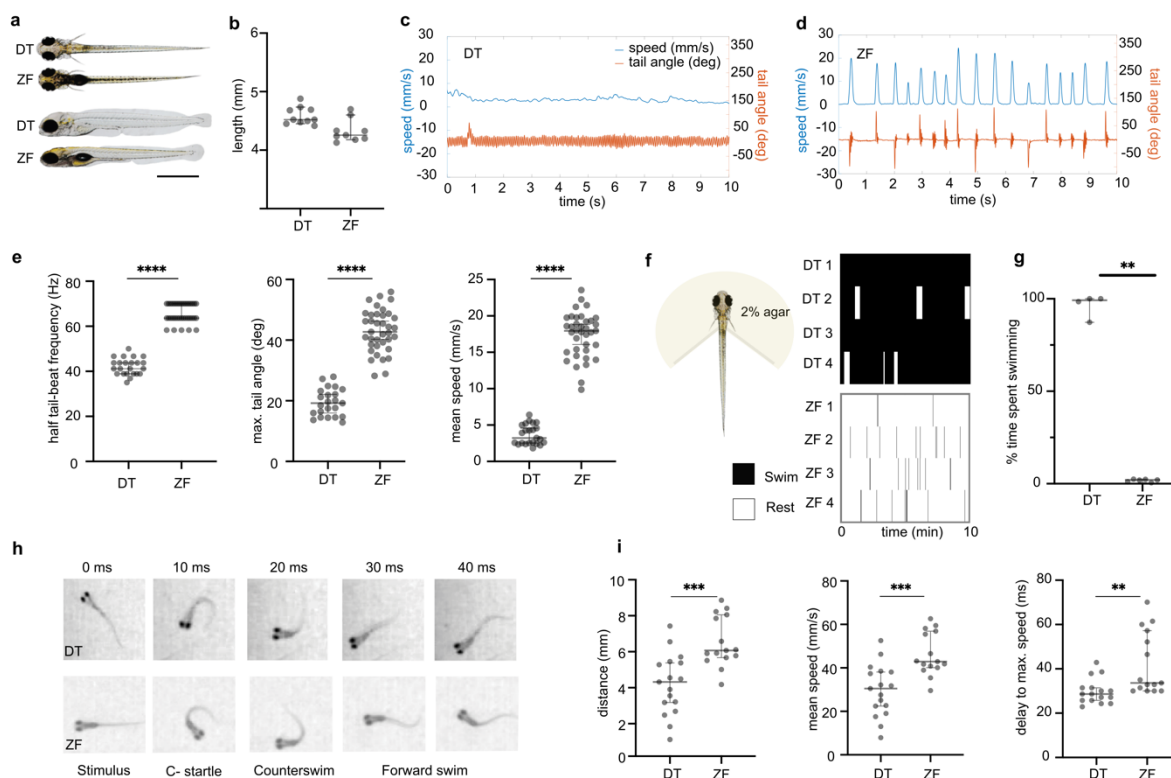
198 role of MLMN in maintenance of the long swim events, we carried out optogenetic stimulation  
199 in ZF *Tg(elavl3:CoChR-eGFP)* which express the opsin CoChR under a pan-neuronal  
200 promoter. We targeted MLMN using 2-photon holographic stimulation with temporal focusing  
201 (Fig. 4f)<sup>35</sup> and observed a reliable increase in swimming following the stimulation (Fig. 4g-h,  
202 Extended Data Movies 4 and 5). MLMN stimulation led to an increase in the mean duration of  
203 bouts and an increase in the frequency of bouts (Fig. 4h), indicating an important role for  
204 MLMN in the maintenance of long swim events. The recruitment of swimming on mere  
205 stimulation of MLMN alone also suggests that this neuronal population also comprises of some  
206 initiation neurons. Interestingly, the discrete swimming patterns of ZF was maintained despite  
207 sustained stimulation of the MLMN, suggesting that this property is embedded downstream,  
208 possibly in the spinal cord of ZF as previously observed for spinalized ZF preparations deprived  
209 of supraspinal inputs<sup>36</sup>. It remains to be further investigated how the long-lasting neuronal  
210 activity is produced in DT. The answer may lie in the intrinsic membrane or network properties  
211 of the identified neurons and warrants further investigation<sup>37,38</sup>.

212 In conclusion, using two closely related fish species, we show that two anatomically similar  
213 brains with conserved features are able to produce different behavioral outputs based on  
214 functional differences in a subset of neurons called MLMN. We also suggest selective pressures  
215 which could have led to the divergence of the swimming pattern. This lays the foundation for  
216 future work to directly compare neuronal circuits and behaviors in vertebrate species, applying  
217 an approach that has been very successfully used in various invertebrate studies<sup>28,39</sup>. This is  
218 particularly interesting to perform in danionin fish as many related species are known and can  
219 be raised in a laboratory setting. With the ability to assign behavioral modules to their  
220 corresponding genetic and neuronal circuit components in ZF (and other danionins), our work  
221 provides a powerful approach in comparative neuroethology to investigate evolution of  
222 behaviors and neuronal circuits in vertebrates.

223

224 **Figures**

225



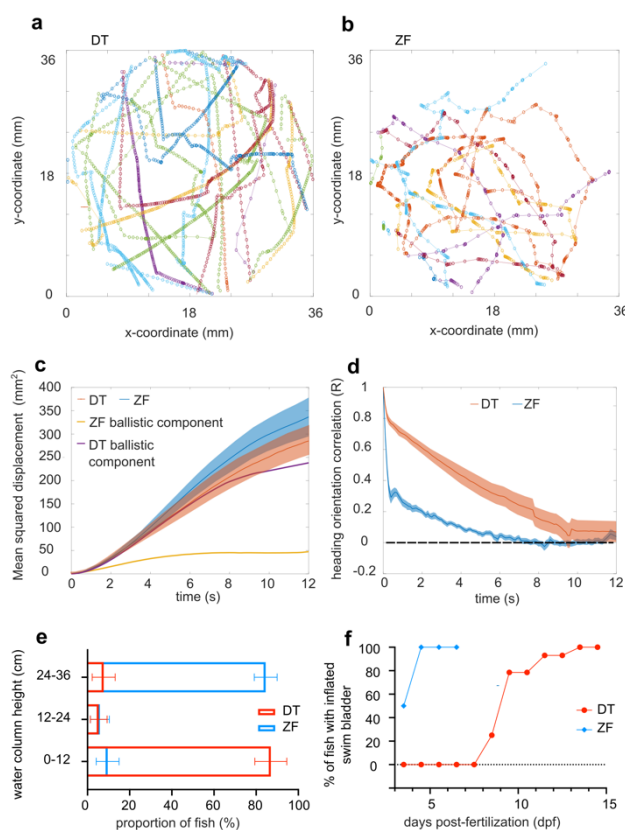
226

227 **Fig. 1: Kinematics of spontaneous swimming, head-embedded swimming and escape**  
 228 **response in DT and ZF.**

229 Larval DT and ZF measure similar in size at 5 dpf. (a) A dorsal and lateral view of DT and ZF  
 230 at 5 dpf is shown. (b) Measurement of body length in 5 dpf DT and ZF falls in a range of 4.1 to  
 231 4.9 mm. (N= 10 DT; N= 9 ZF). (c-d) A comparison of swimming pattern in 6 dpf DT and ZF.  
 232 It demonstrates the continuous swimming pattern in DT with lower speed (cyan) and smaller  
 233 tail angle (orange) when compared to the faster discrete swimming in ZF. (e) Swimming  
 234 kinematics of DT and ZF in a spontaneous swimming assay. DT utilizes lower half tail beat  
 235 frequency (Hz) and lower maximum tail angles (degree) to achieve swimming at lower speeds

236 (mm/s) when compared to ZF (N= 23 DT, n = 494628 half tail beats and N= 37 ZF, n = 202176  
237 half tail beats). (f) Tail movements in head-embedded preparations depicted in raster plots  
238 illustrate the prolonged swims of DT (top) compared to the short bouts of ZF (bottom). (g) The  
239 fraction of time spent actively swimming (% of total acquisition time) is higher in DT compared  
240 to ZF (N=5 DT and N= 6 ZF). (h) Qualitatively, the escape response after a tap stimulus is  
241 highly similar between DT and ZF. The images were acquired at 100 Hz. (i) Although DT  
242 covers a shorter distance at a lower mean speed, the time to achieve the maximum speed is  
243 lower in DT compared to ZF (DT: N=19 fish, n=141 events; ZF: N=15 fish, n=159 events). \*\*  
244  $p < 0.01$ , \*\*\*  $p = 0.001$ , \*\*\*\*  $p < 0.0001$ , Mann-Whitney test. All error bars show 95 % confidence  
245 interval.

246

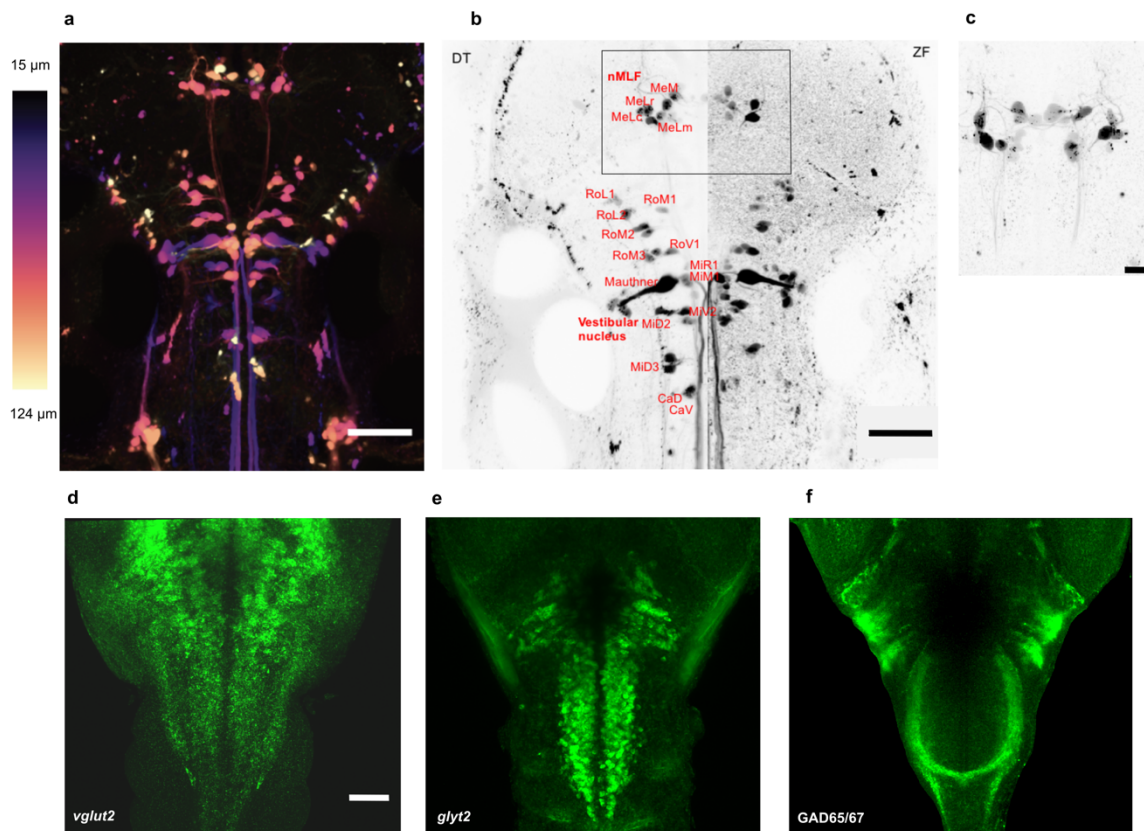


247

248 **Fig. 2: Long-term exploratory kinematics of DT and ZF.**

249 (a) and (b) represent a few tens of swim trajectories depicted in different colors from a single  
250 DT and ZF larva, respectively. (c) Mean squared displacement (MSD) in DT and ZF over time.  
251 The MSD over time for the ballistic component of DT and ZF is also overlapped on the plot.  
252 The ballistic component of the MSD was estimated as:  $MSD_{bat}(t) = \langle \left[ \int_{t_0}^{t_0+t} \mathbf{v} * \mathbf{R}(t' - \right.$   
253  $\left. t_0) \cdot d\mathbf{t}' \right]^2 \rangle_{t_0}$ . The error bars show s.e.m. (d) Decorrelation in heading persistence over time.  
254  $R=1$  indicates a perfect persistence in head direction whereas  $R=0$  corresponds to a dull  
255 randomization. In ZF,  $R$  drops rapidly whereas this drop happens over longer period of time in  
256 DT. Hence, exploratory swimming in DT has a longer ballistic phase. The error bars show  
257 s.e.m. (e) DT larvae occupy the bottom of the water column whereas ZF larvae occupy the top.  
258 ( $N \sim 30$  fish and  $n = 10$  readings in 3 replicates for each fish species). The error bars show 95%  
259 confidence interval. (f) Swim bladder inflation in ZF occurs earlier than in DT. The inflation of  
260 swim bladder in ZF occurs by  $\sim 4-5$  dpf whereas DT inflates their swim bladder between  $\sim 10$   
261 and  $\sim 15$  dpf. Sampled from a growing population of approximately  $N = 30$  DT and 30 ZF.

262



263

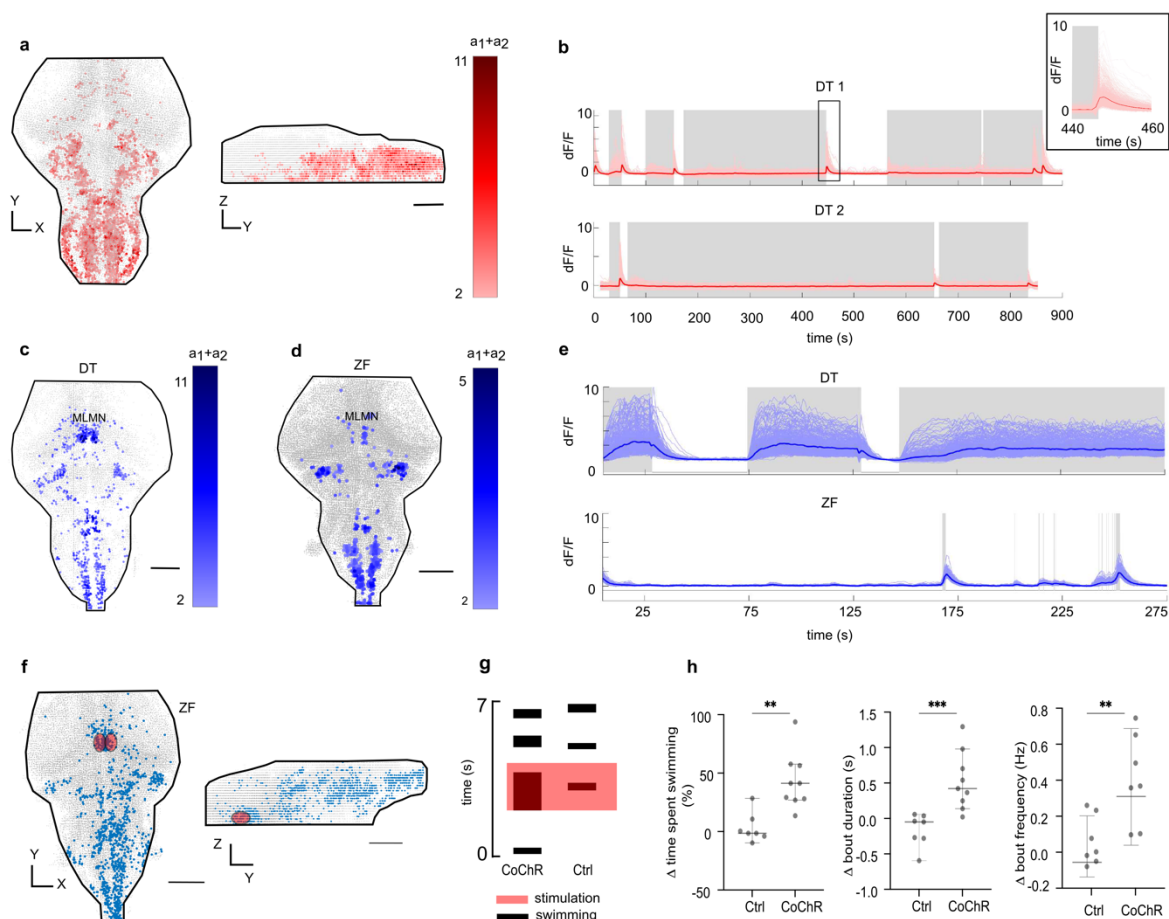
264 **Fig. 3: Distribution of reticulospinal neurons and excitatory and inhibitory neuronal cell**  
 265 **types in the hindbrain of DT and ZF.**

266 (a) Distribution of reticulospinal (RS) neurons in the brainstem of DT. Maximum intensity is  
 267 color coded for depth. Scale bar is 100  $\mu\text{m}$ . (b) Comparison of RS neurons in DT and ZF. A  
 268 cell-to-cell comparison of RS neurons in a maximum intensity projection of RS neurons in DT  
 269 and ZF. The RS neurons in DT are annotated based on the description of RS neurons in ZF.<sup>23,24</sup>  
 270 A high degree of conservation is observed. Scale bar is 100  $\mu\text{m}$ . (c) A closer look at the  
 271 rectangular ROI from (b) in another DT fish. Maximum intensity projection of the nucleus of  
 272 the medial longitudinal fasciculus (nMLF) in another DT fish is shown. Contralateral dendritic  
 273 projections are observed in DT as noted in ZF<sup>23</sup>. Scale bar is 30  $\mu\text{m}$ . Distribution of (d)  
 274 glutamatergic (e) glycinergic and (f) GABAergic neurons in the hindbrain of DT. Performed  
 275 using *in-situ* hybridization (ISH) and immunohistochemistry (IHC). Rostrocaudally running  
 276 striped pattern of these neuronal types is observed in DT as noted in ZF before<sup>25</sup>. Anti-*vglut2a*

277 + anti-*vglut2b* ISH and anti-*glyt2* ISH in (d) and (e), respectively. Anti-GAD65/67 IHC in (f).

278 All images are a maximum intensity projection. Scale bar is 50  $\mu$ m.

279



280

281 **Fig. 4: Neurons correlated with termination of swimming (in DT) and swimming (in DT**  
 282 **and ZF); and holographic stimulation of the identified Mesencephalic Locomotion**  
 283 **Maintenance Neurons (MLMN).**

284 (a) Representative images of stop cells (in red) identified in the DT hindbrain (N=3). (b)

285 represents the activity of the identified stop neurons (in red) with respect to swimming activity

286 (in grey). The inset shows a magnified region around a swim termination event. (c) and (d)

287 show a representative figure of a maximum projection of neuronal correlates of swimming (in

288 blue) identified in the DT and ZF brain, respectively. The nuclei correlated with swimming

289 appear to be conserved between DT (N=4) and ZF (N=4). The MLMN population is labelled.  
290 (e) Neuronal activity of all the swimming correlated neurons in DT compared to the  
291 corresponding neurons' activity in a ZF for a duration of 300 seconds. The activity in the  
292 conserved nuclei in DT is sustained for long durations unlike ZF, correlating with their long  
293 swim events. The grey shaded regions represent active swimming. (f) The region of interest  
294 (ROI) for holographic optogenetic stimulation is illustrated. MLMN population described in  
295 (c) and (d) was first anatomically located under a 2-photon microscope using expression of  
296 CoChR-GFP (in test) or GCaMP6 (in control) as the guidance cue. A holographic stimulation  
297 protocol was then employed in this ROI (see Extended Data Fig. 7). (g) illustrates the result of  
298 the stimulation in a CoChR and Ctrl fish. Swimming activity in CoChR fish is increased during  
299 the holographic stimulation. (h) Change in total swimming time, bout duration and bout  
300 frequency during optogenetic stimulation. The time spent swimming is prolonged in test fish  
301 by the optogenetic stimulation; this increase is caused by both, an increased recruitment of  
302 bouts and an increase in the duration of the bouts. N = 7 Ctrl ZF and 9 CoChR ZF. \*\* p<0.01,  
303 \*\*\* p=0.001, Mann-Whitney test. All error bars show 95 % confidence interval. Scale bars are  
304 100  $\mu$ m.

305

## 306 **Methods**

### 307 **Fish breeding and husbandry**

308 6 days post-fertilization (dpf) zebrafish (ZF) and *Danioella translucida* (DT) larvae were used  
309 for behavioral experiments. For imaging experiments, 5 dpf ZF and DT were used. DT adults  
310 were grown at a water temperature of 25 to 28° C, pH of 6.3 to 8.3 and a conductivity of 250 to  
311 450  $\mu$ S. Adult DT are fed with Gemma Micro 150 (Skretting, USA) (twice a day) and live



312 *Artemia* (once a day). DT are known to spawn in crevices<sup>3</sup>. Hence, 2 to 4 silicone tubes (~ 5  
313 cm long) were added in the adult tanks to aid spawning.

314 The larvae were grown at a density of <50 larvae per 90 cm Petri plate in E3 egg medium  
315 (without methylene blue). For behavioral experiments, at 5 dpf, both larval ZF and DT were  
316 transferred to a 250 ml beaker with 100 ml E3 egg medium (without methylene blue) and fed  
317 with rotifers. They were maintained at 28°C in an incubator until the experiment at 6 dpf. The  
318 DT larvae were more delicate and required careful handling. Resultantly, the number of DT  
319 required to perform each experiment was much larger compared to ZF.

320 All animal procedures (ZF and DT) were performed in accordance with the animal welfare  
321 guidelines of France and the European Union. Animal experimentations were approved by the  
322 committee on ethics of animal experimentation at Institut Curie and Institut de la Vision, Paris.

323

#### 324 **Free-swimming behavioral acquisition, fish tracking and tail segmentation**

325 A high-speed camera (MC1362, Mikrotron-GmbH, Germany) and a Schneider apo-Xenoplan  
326 2.0/35 objective (Jos. Schneider Optische Werke GmbH, Germany) were used to carry out the  
327 free-swimming acquisitions. The resolution of the images were 800 x 800 pixels with 17 pixels  
328 /mm and the acquisition was carried out at 700 Hz. The fish were illuminated with an infrared  
329 LED array placed below the swimming arena. An 850 nm infrared bandpass filter (BP850-35.5,  
330 Midwest Optical Systems, Inc.) was used on the objective to block all the visible light.

331 The behavioral arena was illuminated with visible light at 220 lux which was similar to the light  
332 intensity in the home incubator. The fish were transferred to 35 mm Petri plates and  
333 acclimatized for > 2 hours before the behavioral acquisitions. 23 DT and 37 ZF were tested  
334 with the acquisition lasting for ~ 20 - 30 minutes.

335 Image acquisition, fish tracking and tail segmentation were performed using a custom-written  
336 C# (Microsoft, USA) program. The online tracking of the fish and tail segmentation was carried  
337 out as described earlier elsewhere<sup>40</sup>. Briefly, the following method was performed. A  
338 background was calculated by taking the mode of a set of frames which are separated in time  
339 so that the fish occupies a different position in each frame. This background image was  
340 subtracted from each acquired frame. The subtracted image was smoothed using a boxcar filter.  
341 A manually selected threshold was used to separate the fish from the background. The fish blob  
342 was selected by performing a flood fill starting at the maximum intensity point. The center of  
343 mass of this shape was considered the position of the larva. The middle point on a line joining  
344 the center of mass of each eye was defined as the larva's head position. The direction of the tail  
345 was identified by finding the maximum pixel value on a 0.7 mm diameter circle around the  
346 head position. Then, a center of mass was calculated on an arc centered along this direction.  
347 The angles of ~10 tail segments measuring 0.3 mm were calculated. To do this, successive tail  
348 segments were identified by analyzing the pixel values along a 120-degree arc from the  
349 previous segment. This same algorithm was used for both DT and ZF. The empirically selected  
350 threshold to separate the fish from background was different in the two fish.

351

### 352 **Analysis pipeline for free-swim data**

353 Poor tracking was identified using pixel intensities of the tail segments. The lost frames, if any,  
354 were identified based on a 32-bit timestamp encoded in the first 4 pixels of all the images. These  
355 lost frames are then interpolated and filled with NaN values for the recorded parameters.

356 Discontinuities in turning when the fish turns from 0 to 360 degree or vice versa were corrected.

357 The raw X and Y coordinates were smoothed using the Savitzky Golay digital filter: in  
358 MATLAB (MathWorks, USA), *sgolayfilt* function is used to implement this. A 2<sup>nd</sup> order

359 polynomial fit was employed on a window size of 21 units (30 ms). Displacement was  
360 calculated using these X and Y coordinates of the centroid of the fish.

361 The measure of tail curvature was used to identify the bouts<sup>40</sup>. The first 8 tail segments were  
362 incorporated in the analysis based on the reliability of the tracking as assessed by the raw pixel  
363 intensities. The change in the curvature of the tail was emphasized over local fluctuations by  
364 taking a cumulative sum of the values along the tail. The differences in tail angles were  
365 calculated as we wanted to detect movements. The tail movements were then smoothed using  
366 a boxcar filter of size equivalent to ~14.30 ms. The absolute of the segment angles were then  
367 convolved into a single curvature measure. A maxima/minima filter of 28.6 ms/ 572 ms was  
368 specifically applied to this tail curvature dataset of ZF based on the knowledge of bout and  
369 inter-bout durations available to us. An empirically validated cut-off was used on the convolved  
370 and smoothed tail curvature measure to identify the starts and ends of swim bouts. It is  
371 important to note that in the analysis, only the ‘burst’ phase of ‘burst-and-glide’ swims were  
372 identified in ZF.

373 The 7<sup>th</sup> tail segment was used for calculating tail beat frequency and maximum tail angle. The  
374 trace of the tail segment was smoothed and small gaps (less than 7 ms) in the swim events due  
375 to tracking were interpolated. Swim events with larger gaps were eliminated from the analysis.  
376 Any identified events shorter than 71.5 ms in length, if present, were discarded as well to avoid  
377 artefacts. On the bout-based kinematics, the bout distance, inter-bout duration, mean and  
378 maximum speed, maximum tail angle and tail beat frequency were calculated.

379

### 380 **Half beat based kinematics in ZF and DT**

381 A peak-to-peak half cycle was defined as a half tail beat cycle and this was used for the  
382 kinematic calculations to be able to compare a similar unit of locomotion between the two fish.

383 In ZF: to identify the half-beats, on every swim bout, the absolute of the tail angles was  
384 calculated from the 8<sup>th</sup> segment of the tail and the peaks of tail angle were identified using the  
385 *findpeaks* function in MATLAB. Extended Data Fig. 1a shows this for a swim bout in ZF.

386 In DT: the trace of the tail segment is smoothed using a Savitzky Golay digital filter function  
387 of 3<sup>rd</sup> order with a window size of 50 ms. Small gaps (less than 7 ms) in the tracking were  
388 interpolated. Using *bwlabel* function in MATLAB on a binary matrix of good/ bad tracking, all  
389 continuous stretches of good tracking were labelled. From this, only the stretches longer than  
390 35 frames (or 50ms) were selected for further analysis to avoid small tracking artefacts if any.  
391 On these identified stretches, half beats were identified as mentioned above for ZF.

392 On every half beat in both the fishes, the following kinematic parameters were calculated:  
393 duration, distance, mean and maximum speed, maximum tail angle and half beat frequency.  
394 The 8<sup>th</sup> tail segment was used for calculating tail beat frequency and max tail angle.

395

### 396 **Head-embedded swimming**

397 A high-speed camera (MC4082, Mikrotron-GmbH, Germany) with a Navitar Zoom 7000 macro  
398 lens was used to carry out the head-embedded acquisitions. The resolution of the images were  
399 400 x 400 pixels with 75 pixels /mm and the temporal resolution of the acquisition was 100 or  
400 250 Hz. The fish were illuminated with an infrared LED array placed below the swimming  
401 arena. An 850 nm infrared bandpass filter (BP850-35.5, Midwest Optical Systems, Inc.) was  
402 used on the objective to block all the visible light.

403 6 dpf DT (n=4) and ZF (n=6) were embedded in 0.5 ml of 1.5% agarose. For ZF, nacre incross  
404 fish were used. The agarose covered the head up to the pectoral fins. Each fish was acclimatized  
405 for at least 90 minutes before acquisition. Recordings lasted for 10-20 minutes per fish. The  
406 head-embedded videos were primarily used to determine the amount of time spent in

407 swimming. The tail tracking was performed manually to identify the swimming and resting  
408 time periods. The duration of swimming was normalized to the total length of the acquisition  
409 and reported as a percentage of the total duration of acquisition.

410

### 411 **Tap-induced escape behavior**

412 An Arduino controlled solenoid was added to the free-swimming behavioral set-up. The  
413 Arduino was triggered from the image acquisition program written in C# (Microsoft, USA).  
414 When triggered, the solenoid would hit the surface of the arena from the bottom and cause the  
415 fish to escape in response to this stimulus. The trigger was only initiated if the fish was not at  
416 the edges of the Petri dish and if there was an inter-stimulus interval of at least 50 seconds  
417 between two consecutive trials. The delay between the trigger onset and the delivery of the  
418 solenoid on the arena was estimated and incorporated in the analysis to calculate an accurate  
419 reaction time. 19 DT (n=141 trials) and 15 ZF (n=159 trials) were tested in the assay.  
420 Acquisition at 700 Hz was used for the analysis. However, the illustrated images were captured  
421 at 100 Hz.

422 To analyze the escape kinematics, the peak escape velocities were identified in a window of  
423 approx. 450 ms after the stimulus delivery. A peak speed was considered as at least 2 times the  
424 peak speed during free-swimming (9.25mm/s and 42.5 mm/s for DT and ZF, respectively). In  
425 case of multiple peak escape velocities in the window, only the first one was considered. Now  
426 a 140 ms region of interest was selected around the peak speed to include 40 ms before the peak  
427 and 100 ms after the peak as shown in Extended Data Fig. 2 for a ZF. The region of interest  
428 was empirically decided after exploring many trials across both the fish species. Mean speed,  
429 total distance covered and the delay to reach the peak speed after the stimulus delivery – these  
430 parameters were computed for all the trials in each fish.

431 The major differences in the processing pipeline from the free-swimming analysis pipeline were  
432 as follows. The X/Y displacement vectors were further filtered using a zero-phase digital  
433 filtering (*filtfilt* function in MATLAB) with a filter size of 11 ms to identify the peak escape  
434 velocities. Kinematics were neither calculated on half beats nor bouts, but on the custom  
435 defined 140 ms window for a better comparison of the escape events in the two species of fish.

436

### 437 **Mean squared displacement (MSD) and reorientation analysis**

438 Information on X/Y- coordinates was used to compute the Mean squared displacement (MSD)  
439 and decorrelation in heading orientation (R) over time. A Savitsky-Golay filter was applied on  
440 the X and Y traces to fit a 2<sup>nd</sup> order polynomial on a 200 ms window. The filtered trajectories  
441 were then downsampled to 70 Hz. For each fish, discrete continuous trajectories were identified  
442 in a circular region of interest of radius 18mm to mitigate border-induced bias. These  
443 trajectories were used for the computation.

444 The time-evolution of MSD and R were calculated at every 100 ms time-step and averaged over  
445 all trajectories for each animal. To compute R, we extracted at each time  $t$  a unit vector  $\mathbf{u}(t)$   
446 aligned along the fish displacement  $[dx, dy]$  calculated over a 1s time window. Notice that this  
447 vector was only calculated if the fish had moved by at least 0.5 mm in this time period. The  
448 heading decorrelation over a period  $\Delta t$  was then computed as  $R(\Delta t) = \langle \mathbf{u}(t) \cdot \mathbf{u}(t + \Delta t) \rangle_t$ . This  
449 function R quantifies the heading persistence over a given period:  $R=1$  corresponds to a perfect  
450 maintenance of the heading orientation, whereas  $R=0$  corresponds to a complete randomization  
451 of the orientations. The MSD and R values were plotted over time for DT (n=23 fish) and ZF  
452 (n=37 fish).

453

454 **Quantification of depth preference**

455 Three vertical glass cylinders with 36 cm water height were used in this experiment. 6 dpf ZF  
456 larvae (n=30 per cylinder) were added to three cylinders. 6 dpf DT larvae (n=30 per cylinder)  
457 were added to another three cylinders.

458 The cylinders were considered as consisting of three sections and marked accordingly: the  
459 bottom 12 cm, middle 12 cm and the top 12 cm. The number of fish in each section of the  
460 column was manually counted once every hour for 10 hours. Only the fish that were swimming  
461 normally were considered for the enumeration. This was used to calculate the average  
462 normalized fish density in every section of the water column.

463

464 **Quantification of body length and swim bladder inflation**

465 Body length was measured in 5 dpf larvae of the two species (n = 10 for DT and n = 9 for ZF).  
466 Pictures of the larvae were captured using an AxioCam MR3 camera. The magnification of the  
467 optics was noted and the physical dimension of the camera pixel was used to calculate the pixel  
468 size in  $\mu\text{m}$  as follows: pixel size = (260/magnification) x binning factor.

469 To quantify swim bladder inflation, from a population of growing larvae (3 dpf to 15 dpf), five  
470 or more larvae were sampled for each age and the proportion of larvae with inflated swim  
471 bladder was quantified. The sampling was performed from a growing population of  
472 approximately N = 30 DT and 30 ZF. A moving averaging was performed using a window size  
473 of two units to smoothen the curve and the swim bladder inflation results were reported from  
474 3.5 to 14.5 days.

475

476 **Whole-mount *in-situ* hybridization (ISH)**

477 To generate anti-sense probes, DNA fragments were obtained by PCR using Phusion™ High-  
478 Fidelity DNA Polymerase (Thermo Scientific™) and the following primers (5' → 3')<sup>41</sup>: vglut2a  
479 (forward primer: *AGTCGTCTAGCCACAACCTC*; reverse primer:  
480 *CACACCATCCCTGACAGAGT*), vglut2b or *slc17a6b* (forward primer:  
481 *GCAATCATCGTAGCCAACTTC*; reverse primer: *ACTCCTCTGTTTTCTCCATC*), glyt2 or  
482 *slc6a5* (forward primer: *TGGAAGGATGCTGCTACACA*; reverse primer:  
483 *TGACCATAAGCCAGCCAAGA*) and gad67 or *gad1b* (forward primer:  
484 *CCTTCCTCCTCGGCGATTGA*; reverse primer: *GGCTGGTCAGAGAGCTCCAA*). Total  
485 cDNA for ZF and DT were used as a template. PCR fragments were cloned into the pCRII-  
486 TOPO vector (Invitrogen) according to manufacturer's instructions. All plasmids used were  
487 sequenced for confirmation.

488 Digoxigenin RNA-labeled or Fluorescein RNA-labeled probes were transcribed *in vitro* using  
489 the RNA Labeling Kit (Roche Diagnostics Corporation) according to manufacturer's  
490 instructions. Dechorionated embryos at the appropriate developmental stages were fixed in  
491 fresh 4% paraformaldehyde (PFA) in 1X phosphate buffered saline (pH 7.4) and 0.1% Tween  
492 20 (PBST) for at least 4 hours at room temperature or overnight at 4° C. Following this, the  
493 samples were preserved in methanol at -20° C until the *in-situ* experiments described below.  
494 Whole-mount digoxigenin (DIG) *in-situ* hybridization was performed according to standard  
495 protocols<sup>42</sup>. A protease-K (10 µg/mL) treatment was performed depending on the age and  
496 species of the sample (90 minutes and 120 minutes for 5 dpf DT and ZF, respectively). The  
497 samples were imaged on a stereoscope with AxioCam MR3 camera.

498



499 **Vibratome section**

500 The whole-mount samples were embedded in gelatin/albumin with 4% of Glutaraldehyde and  
501 sectioned at 20  $\mu\text{m}$  thickness on a vibratome (Leica, VT1000 S vibrating blade microtome).  
502 The sections were mounted in Fluoromount Aqueous Mounting Medium (Sigma) before  
503 imaging.

504

505 **Whole-mount Fluorescence *in-situ* hybridizations (FISH)**

506 The samples stored in methanol at  $-20^{\circ}\text{C}$  were rehydrated by two baths of 50% methanol/PBST  
507 followed by two baths of PBST. This was incubated for 10 min in a 3%  $\text{H}_2\text{O}_2$ , 0.5% KOH  
508 solution, then rinsed in 50% methanol/ 50% water and again dehydrated for 2 hours in 100%  
509 methanol at  $-20^{\circ}\text{C}$ . Samples were rehydrated again by a series of methanol baths from 100% to  
510 25% in PBST, and washed two times in PBST. This was followed by an age and species  
511 dependent treatment of proteinase-K (10  $\mu\text{g}/\text{mL}$ ) at room temperature. At 5 dpf, DT and ZF  
512 underwent treatment of proteinase-K for 90 and 120 minutes, respectively.

513 Following this, the samples were again fixed in 4% PFA/PBST. After 2 hours of pre-  
514 hybridization in HY4 buffer at  $68^{\circ}\text{C}$ , hybridization with fluorescein-labelled probes (40ng  
515 probes in 200  $\mu\text{l}$  HY4 buffer) was performed overnight at  $68^{\circ}\text{C}$  with gentle shaking. Embryos  
516 were rinsed and blocked in TNB solution (2% blocking solution (Roche) in TNT) for 2 hours  
517 at room temperature. This was then incubated overnight with Fab fragments of anti-Fluo-POD  
518 (Roche) diluted 1:50 in TNB. For signal revelation, embryos were washed with 100  $\mu\text{l}$   
519 Tyramide Signal Amplification (TSA, PerkinElmer) solution and incubated in the dark with  
520 Fluorescein (FITC) Fluorophore Tyramide diluted 1:50 in TSA. The signal was then followed  
521 for 30 minutes for *glyt* and 1 hour for *vgult2b* until a strong signal was observed. After which,

522 the reactions were stopped by 5 washes with TNT, and incubated for 20 minutes with 1% H<sub>2</sub>O<sub>2</sub>  
523 in TNT. All the steps after Fluorescein (FITC) incubation were processed in the dark.

524

### 525 **Immuno-histochemistry**

526 Briefly, the whole mount embryos were washed twice in TNT solution. Subsequently, they  
527 were blocked for 1 hour at room temperature in 10% Normal Goat Serum (Invitrogen) and 1%  
528 DMSO in TNT solution. Rabbit GAD65/67 primary antibody (AbCam) diluted 1/5000 in 0.1%  
529 blocking solution was incubated overnight at 4°C. The Alexa Fluor 635 secondary antibody  
530 goat anti-rabbit IgG (1/500) (Life Technologies) was added in 0.1% blocking solution and  
531 incubated overnight at 4°C. After 5 washes in PBST buffer, microscopic analysis was  
532 performed.

533

### 534 **Confocal imaging of the whole brain FISH/IHC samples**

535 To image the whole brain *in-situ* hybridization and immunohistochemistry samples, we used  
536 Zeiss LSM 780, LSM 800 and LSM 880 confocal microscopes with a 10x or 40x objective  
537 using appropriate lasers and detection schemes suitable to the labelled sample. Whole brain  
538 images were acquired in tiles and stitched together using the stitching algorithm available in  
539 Zeiss ZEN blue and ZEN black. The images are shown as maximum intensity projections  
540 created on imageJ. In GAD65/67 IHC, non-specific blobs of signal likely originating from  
541 residual dye left on the skin after the washing step was removed using image processing in the  
542 representative image.

543

#### 544 **Retrograde labelling of reticulospinal (RS) neurons**

545 A solution containing 10% w/v Texas Red dextran (TRD, 3,000 MW, Invitrogen) in water was  
546 pressure injected in the spinal cord (between body segment 7 to 14) of 4dpf ZF and DT. In DT,  
547 this method resulted in less efficient labeling of the RS neurons. The best results were obtained  
548 by cutting the tail beyond segment 14th with fine scissors and pressure injecting the TRD in the  
549 exposed spinal cord. After the labeling, the fish were allowed to recover in E3 egg medium for  
550 24 hours at 28° C.

551 At 5dpf, the surviving injected larvae were anaesthetized with 0.02% Tricaine (MS-222,  
552 Sigma), mounted in 1.5% low melting point agarose and imaged under a VIVO 2-photon  
553 microscope (3I, Intelligent Imaging Innovations Ltd). Labelling was often sparse and varied  
554 among the injected fish which survived to 5dpf (n=4 fish per species). Maximum intensity  
555 projection images of the reticulospinal neurons in ZF and DT is shown from the animals where  
556 almost all the RS neurons were labelled. RS neurons in the DT brain were annotated based on  
557 their anatomical similarity to the ones in ZF<sup>23</sup>.

558

#### 559 **Generation of pan-neuronal calcium sensor *Tg(elavl3-H2B:GCaMP6s)* line**

560 To generate *Tg(elavl3:H2B-GCaMP6s)* DT fish, 6 ng/μl of the plasmid and 25 ng/μl of Tol2  
561 was used. Injections were performed in embryos which were less than or equal to 4-cell stage.  
562 The injection was performed free-hand as DT lay eggs in clutches. Tol2-elavl3-H2B-GCaMP6s  
563 plasmid was a gift from Misha Ahrens (Addgene plasmid # 59530;  
564 <http://n2t.net/addgene:59530>; RRID: Addgene\_59530)<sup>44</sup>.

565

#### 566 **Light sheet microscopy**

567 Transgenic DT and ZF expressing H2B-GCaMP6s under the *elavl3* promoter were utilized. The  
568 GCaMP is nuclear tagged, so its expression is limited to the nucleus which makes it easier for  
569 segmentation of the neurons. The fish were embedded in a capillary with 2.5% agar. The tail  
570 was freed and recorded simultaneously to extract a readout of the spontaneous swimming  
571 behavior. Before each recording, the embedded fish were acclimatized to the recording chamber  
572 with the blue laser switched on for at least 10 minutes. The scanning objective was lateral and  
573 the beam entered from the left side of the fish and the detection objective was placed upright  
574 on the top. Both the objectives were moved with a piezo so that the light sheets were always in  
575 the focal plane of the detection objective. Average laser power was at 0.05 mW. Approximately  
576 280  $\mu\text{m}$  of the brain volume was imaged in each fish. Brain imaging was carried out at  
577 approximately 1 Hz (1 whole brain volume / s) and the tail movement was acquired at  $\sim$  40-80  
578 Hz. Each acquisition lasted for  $\sim$  20 minutes.

579

### 580 **Image processing and analysis pipeline for whole-brain light-sheet data**

581 For ZF and DT, image processing was performed offline using MATLAB. Based on visual  
582 inspection, if needed, image drift was corrected by calculating the cross-correlation on a  
583 manually selected region of interest (ROI). The dx and dy values employed to correct the drift  
584 in this ROI were extrapolated to the whole stack. Brain contour was manually outlined on mean  
585 greystack images for each layer. Background value for each layer was estimated from the  
586 average intensity of pixels outside the brain contour. The segmentation procedure consisted of  
587 a regression with a Gaussian regressor convolved with the same Gaussian regressor. The result  
588 was regressed another time with the same regressor. Baseline and fluorescence were calculated  
589 for each neuron identified by the segmentation. The fluorescence  $F(t)$  signal was extracted by  
590 evaluating the mean intensity across the pixels within each neuron. The tail tracking was  
591 performed manually on the tail acquisitions to identify active and inactive time periods. For ZF,

592 the baseline was calculated by the running average of the 10th percentile of the raw data in  
593 sliding windows of 50 seconds. For DT, the baseline for identifying neurons correlated with  
594 swim and stop events was calculated as the 10th percentile of the raw data within each inactive  
595 period defined as the time period between 5 seconds after the end of a swim event and 3 seconds  
596 before the beginning of the next swim event (from tail acquisition data). The baseline values  
597 for the active periods were interpolated using the values in the inactive periods. For both ZF  
598 and DT, the relative variation of fluorescence intensity  $dF/F$  was calculated as  $dF/F = (F(t) -$   
599 baseline) / (baseline-background).

600 For both ZF and DT, neurons from the more rostral part of the brain were removed (y  
601 coordinates between  $y_{\max} - 10$  um and  $y_{\max}$ ) because of  $dF/F$  artefact due to image border. A  
602 multi-linear regression was performed using the classical normal equations. In DT, this was  
603 performed on  $dF/F$  for the whole duration of the experiment and in ZF, on  $dF/F$  for a manually  
604 selected time period with many well isolated swim bouts. The analysis determines the best-fit  
605 coefficient  $\beta$  to explain the neuronal data (y) by the linear combination  $y = \sum \beta_j * x_j + \beta_o$ ,  
606 where  $x_j$  is the regressor. For ZF, a constant regressor and a swim maintenance regressor (based  
607 on the tail acquisition data) were used. For DT, four regressors were used: constant, swim  
608 maintenance, swim onset and swim offset. The onset and offset regressors were obtained from  
609 the initiation and termination of swim events (based on the tail acquisition data) with a time  
610 window of -3 seconds to +1 second around the initiation/ termination event. Swim maintenance,  
611 onset and offset regressors were convolved with a single exponential of 3.5 seconds decay time  
612 which approximates the H2B-GCaMP6s response kernel in ZF<sup>45</sup>. T-scores were computed for  
613 every neuron/regressor combination. We could reliably find neurons highly correlated with  
614 swim maintenance and termination events as shown in the results.

615

616 **Brain registration**

617 We used the Computational Morphometry ToolKit CMTK  
618 (<http://www.nitrc.org/projects/cmtk/>) to compute and average the morphing transformation  
619 from high resolution brain stacks (184 layers and 1  $\mu\text{m}$  z-resolution; 1-photon imaging) to create  
620 a common brain for the *Tg(elavl3:H2B:GCaMP6s)* DT line. All the calcium imaging results  
621 were mapped to this reference brain. To compare neuronal populations across different brain  
622 samples, we calculated the spatial densities of the considered clusters by using the Kernel  
623 Density Estimation (KDE) with a Gaussian kernel with a bandwidth of 12.8  $\mu\text{m}$ . Discrete  
624 cluster densities were determined for all points of an inclusive common 3D rectangular grid  
625 with an isotropic resolution of 5  $\mu\text{m}$ .

626

627 **Optogenetic stimulation**

628 5 to 7dpf ZF were head-embedded in a Petri dish with 2% agarose and the tail was freed to  
629 move. After a period of acclimatization, fish were placed under a custom made 2-photon (2P)  
630 microscope capable of 2P scanning imaging and 2P holographic patterned illumination<sup>46</sup>. The  
631 holographic optical path is analogous to the one described in a previously published work<sup>47</sup>.  
632 Briefly, the use of fixed phase mask, a diffraction grating and liquid crystal spatial light  
633 modulator allows the generation of multiple illumination spots distributed in 3 dimensions<sup>47</sup>.  
634 Additionally, an inverted compact microscope and an infrared LED (780 nm) were placed  
635 below the Petri dish to record the tail movements. 2P scanning imaging of *Tg(elavl3:CoChR-*  
636 *eGFP)* and *Tg(elavl3:H2B-GCaMP6s/6f)* (control) was first performed to locate the MLMN in  
637 the midbrain. To target the MLMN population, we defined a holographic illumination pattern  
638 composed of multiple identical holographic spots distributed over different x-y-z locations.  
639 Each spot has a lateral diameter of 12  $\mu\text{m}$  and an axial FWHM  $\approx$  10 $\mu\text{m}$ . On the x-y plane, the

640 targeted surface is covered by the generation of 10 holographic spots, then this pattern is  
641 reproduced over 3 different planes to adjust the axial extension of the excitation volume  
642 (Extended Data Fig.7). The resulting excitation region corresponds approximately to an  
643 ellipsoid of 40-50-70  $\mu\text{m}$  (x-y-z axis, respectively), matching the size of the MLMN in each  
644 hemisphere (see Fig. 4 f). Neurons in these regions were photo-stimulated by 2P excitation with  
645 the following protocol: 10 ms pulses at 10Hz were delivered for 2 s and repeated 3 times with  
646 30 s intervals between repetitions. The effective excitation light intensity varied from 25 to 40  
647  $\mu\text{W}/\mu\text{m}^2$  and was delivered through a 40x objective (N40X-NIR,0.8 NA,Nikon) by an  
648 amplified fiber laser at 1040 nm (Satsuma,Amplitude System), suitable to efficiently excite  
649 CoChR opsin<sup>48</sup>. Simultaneous recording of the tail movement was performed on a CMOS  
650 camera (MQ013MG-ON Ximea) at a frame rate of 33Hz. For analysis, the tail tracking was  
651 performed manually with the respect to the periods of stimulation. We extracted three  
652 swimming parameters during both, spontaneous swimming and stimulation protocol: bout  
653 duration, bout frequency and proportion of time spent swimming. The increase or decrease in  
654 the mean value of these parameters during the stimulation protocol for each animal is  
655 represented in Fig. 4h.

656

## 657 **Statistical methods**

658 **Behavior data:** All the averaged values per fish were prepared in MATLAB 2017b  
659 (Mathworks) and statistical tests between the populations were carried out in Prism 8  
660 (GraphPad). Mann-Whitney test by ranks was performed in all cases where the dataset did not  
661 follow a normal distribution.

662 **Light-Sheet imaging data:** To characterize highly responsive neurons for a specific regressor,  
663 the regression coefficient and t-score distributions were first fitted with a Gaussian model ( $\mu_{\text{dist}}$ ,  
664  $\sigma_{\text{dist}}$ ) to estimate a sub-distribution responsible for noise (neurons that do not correlated well

665 with the regressor). These sub-distributions, defined as the maximum distribution  $\pm \sigma_{\text{dist}}$ , were  
666 then fitted again with a Gaussian model ( $\mu_{\text{noise}}$ ,  $\sigma_{\text{noise}}$ ). The highly responsive neurons were  
667 defined as neurons with both, a regression coefficient higher than regression threshold<sub>coefficient</sub>  
668  $= \mu_{\text{noise coefficient}} + 3 \sigma_{\text{noise coefficient}}$  (or threshold<sub>coefficient</sub>  $= \mu_{\text{noise coefficient}} + 4 \sigma_{\text{noise coefficient}}$ ) and a  
669 t-score higher than t-score threshold<sub>t-score</sub>  $= \mu_{\text{noise t-score}} + 3 \sigma_{\text{noise t-score}}$  (or threshold<sub>coefficient</sub>  $=$   
670  $\mu_{\text{noise t-score}} + 4 \sigma_{\text{noise t-score}}$ ). To quantify the responsiveness of highly correlated neurons, a score  
671 was created for each neuron based on the sum of the regression coefficient normalized by the  
672 regression threshold<sub>coefficient</sub> ( $a_1$ ) and the t-score normalized by the t-score threshold<sub>t-score</sub> ( $a_2$ ).  
673 The higher the score, the more responsive is the neuron.

674

## 675 **References**

- 676 1. Katz, P. S. & Hale, M. E. *Evolution of Motor Systems. Neurobiology of Motor Control:*  
677 *Fundamental Concepts and New Directions* (2017). doi:10.1002/9781118873397.ch6
- 678 2. Roberts, T. R. *Danionella translucida*, a new genus and species of cyprinid fish from  
679 Burma, one of the smallest living vertebrates. *Environ. Biol. Fishes* **16**, 231–241  
680 (1986).
- 681 3. Schulze, L. *et al.* Transparent *Danionella translucida* as a genetically tractable  
682 vertebrate brain model. *Nat. Methods* **15**, 977–983 (2018).
- 683 4. Penalva, A. *et al.* Establishment of the miniature fish species *Danionella translucida* as  
684 a genetically and optically tractable neuroscience model. *bioRxiv* 444026 (2018).  
685 doi:10.1101/444026
- 686 5. Britz, R., Conway, K. W. & Rüber, L. Spectacular morphological novelty in a  
687 miniature cyprinid fish, *Danionella dracula*. *Proc. R. Soc. B Biol. Sci.* **276**, 2179–2186  
688 (2009).



- 689 6. Conway, K. W., Kubicek, K. & Britz, R. Extreme evolutionary shifts in developmental  
690 timing establish the miniature *Danionella* as a novel model in the neurosciences. *Dev.*  
691 *Dyn.* **280** (2020). doi:10.1002/dvdy.280
- 692 7. Parichy, D. M. Advancing biology through a deeper understanding of zebrafish  
693 ecology and evolution. *Elife* **4**, (2015).
- 694 8. Müller, U. K. & Van Leeuwen, J. L. Swimming of larval zebrafish: Ontogeny of body  
695 waves and implications for locomotory development. *J. Exp. Biol.* **207**, 853–868  
696 (2004).
- 697 9. Van Leeuwen, J. L., Voesenek, C. J. & Müller, U. K. How body torque and Strouhal  
698 number change with swimming speed and developmental stage in larval zebrafish. *J. R.*  
699 *Soc. Interface* **12**, (2015).
- 700 10. Budick, S. A. & O'Malley, D. M. Locomotion of larval zebrafish. *J. Exp. Biol.* **203**,  
701 2565–2579 (2000).
- 702 11. Berg, H. C. & Brown, D. A. Chemotaxis in *Escherichia coli* analysed by three-  
703 dimensional tracking. *Nature* **239**, 500–504 (1972).
- 704 12. Watari, N. & Larson, R. G. The hydrodynamics of a run-and-tumble bacterium  
705 propelled by polymorphic helical flagella. *Biophys. J.* **98**, 12–17 (2010).
- 706 13. Shukla, R. & Bhat, A. Morphological divergences and ecological correlates among  
707 wild populations of zebrafish (*Danio rerio*). *Environ. Biol. Fishes* **100**, 251–264  
708 (2017).
- 709 14. Boehrer, B. & Schultze, M. Stratification of lakes. *Rev. Geophys.* **46**, 1–27 (2008).
- 710 15. Davis, J. C. Minimal Dissolved Oxygen Requirements of Aquatic Life with Emphasis  
711 on Canadian Species: a Review. *J. Fish. Res. Board Canada* **32**, 2295–2332 (1975).

- 712 16. Bagatto, B., Pelster, B. & Burggren, W. W. Growth and metabolism of larval zebrafish:  
713 Effects of swim training. *J. Exp. Biol.* **204**, 4335–4343 (2001).
- 714 17. Green, M. H., Ho, R. K. & Hale, M. E. Movement and function of the pectoral fins of  
715 the larval zebrafish (*Danio rerio*) during slow swimming. *J. Exp. Biol.* **214**, 3111–3123  
716 (2011).
- 717 18. Weihs, D. Respiration and depth control as possible reasons for swimming of northern  
718 anchovy, *Engraulis mordax*, yolk-sac larvae. *Fish. Bull.* **78**, (1980).
- 719 19. Denton, E. J. & Marshall, N. B. The buoyancy of bathypelagic fishes without a gas-  
720 filled swimbladder. *J. Mar. Biol. Assoc. United Kingdom* **37**, 753–767 (1958).
- 721 20. Kimura, Y. *et al.* Hindbrain V2a Neurons in the Excitation of Spinal Locomotor  
722 Circuits during Zebrafish Swimming. *Curr. Biol.* **23**, 843–849 (2013).
- 723 21. Bouvier, J. *et al.* Descending Command Neurons in the Brainstem that Halt  
724 Locomotion. *Cell* **163**, 1191–1203 (2015).
- 725 22. Juvin, L. *et al.* A Specific Population of Reticulospinal Neurons Controls the  
726 Termination of Locomotion. *Cell Rep.* **15**, 2377–2386 (2016).
- 727 23. Kimmel, C. B., Powell, S. L. & Metcalfe, W. K. Brain neurons which project to the  
728 spinal cord in young larvae of the zebrafish. *J. Comp. Neurol.* **205**, 112–127 (1982).
- 729 24. Orger, M. B., Kampff, A. R., Severi, K. E., Bollmann, J. H. & Engert, F. Control of  
730 visually guided behavior by distinct populations of spinal projection neurons. **11**, 327–  
731 333 (2008).
- 732 25. Higashijima, S. I., Mandel, G. & Fetcho, J. R. Distribution of prospective  
733 glutamatergic, glycinergic, and gabaergic neurons in embryonic and larval zebrafish. *J.*  
734 *Comp. Neurol.* **480**, 1–8 (2004).

- 735 26. Koyama, M., Kinkhabwala, A., Satou, C., Higashijima, S. I. & Fetcho, J. Mapping a  
736 sensory-motor network onto a structural and functional ground plan in the hindbrain.  
737 *Proc. Natl. Acad. Sci. U. S. A.* **108**, 1170–1175 (2011).
- 738 27. Kinkhabwalaa, A. *et al.* A structural and functional ground plan for neurons in the  
739 hindbrain of zebrafish. *Proc. Natl. Acad. Sci. U. S. A.* **108**, 1164–1169 (2011).
- 740 28. Newcomb, J. M., Sakurai, A., Lillvis, J. L., Gunaratne, C. A. & Katz, P. S. Homology  
741 and homoplasmy of swimming behaviors and neural circuits in the Nudipleura  
742 (Mollusca, Gastropoda, Opisthobranchia). *Proceedings of the National Academy of*  
743 *Sciences of the United States of America* **109**, 10669–10676 (2012).
- 744 29. Chen, T.-W. *et al.* Ultra-sensitive fluorescent proteins for imaging neuronal activity.  
745 **499**, (2013).
- 746 30. Perrins, R., Walford, A. & Roberts, A. Sensory Activation and Role of Inhibitory  
747 Reticulospinal Neurons that Stop Swimming in Hatchling Frog Tadpoles. *J. Neurosci.*  
748 **22**, 4229–4240 (2002).
- 749 31. Severi, K. E. *et al.* Neural Control and Modulation of Swimming Speed in the Larval  
750 Zebrafish. *Neuron* **83**, 692–707 (2014).
- 751 32. Dunn, T. W. *et al.* Brain-wide mapping of neural activity controlling zebrafish  
752 exploratory locomotion. *Elife* **5**, 1–29 (2016).
- 753 33. Abdelfattah, A. S. *et al.* Bright and photostable chemigenetic indicators for extended in  
754 vivo voltage imaging. *Science (80-. )*. **365**, 699–704 (2019).
- 755 34. Thiele, T. R., Donovan, J. C. & Baier, H. Descending Control of Swim Posture by a  
756 Midbrain Nucleus in Zebrafish. *Neuron* **83**, 679–691 (2014).
- 757 35. Chen, I. W., Papagiakoumou, E. & Emiliani, V. Towards circuit optogenetics. *Current*

- 758 *Opinion in Neurobiology* **50**, 179–189 (2018).
- 759 36. Wiggin, T. D., Anderson, T. M., Eian, J., Peck, J. H. & Masino, M. A. Episodic  
760 swimming in the larval zebrafish is generated by a spatially distributed spinal network  
761 with modular functional organization. *J. Neurophysiol.* **108**, 925–934 (2012).
- 762 37. Antri, M., Fénelon, K. & Dubuc, R. The contribution of synaptic inputs to sustained  
763 depolarizations in reticulospinal neurons. *J. Neurosci.* **29**, 1140–1151 (2009).
- 764 38. Li, W. C., Soffe, S. R., Wolf, E. & Roberts, A. Persistent responses to brief stimuli:  
765 Feedback excitation among brainstem neurons. *J. Neurosci.* **26**, 4026–4035 (2006).
- 766 39. Seeholzer, L. F., Seppo, M., Stern, D. L. & Ruta, V. Evolution of a central neural  
767 circuit underlies *Drosophila* mate preferences. *Nature* **559**, 564–569 (2018).
- 768 40. Marques, J. C., Lackner, S., Félix, R. & Orger, M. B. Structure of the Zebrafish  
769 Locomotor Repertoire Revealed with Unsupervised Behavioral Clustering. *Curr. Biol.*  
770 **28**, 181-195.e5 (2018).
- 771 41. Kadobianskyi, M., Schulze, L., Schuelke, M. & Judkewitz, B. Hybrid genome  
772 assembly and annotation of *Danionella translucida*. *Sci. Data* **6**, 1–7 (2019).
- 773 42. Thisse, C. & Thisse, B. High-resolution in situ hybridization to whole-mount zebrafish  
774 embryos. *Nat. Protoc.* **3**, 59–69 (2008).
- 775 43. Kimmel, C. B., Powell, S. L. & Metcalfe, W. K. Brain Neurons Which Project to the  
776 Spinal Cord in Young Larvae of the Zebrafish. **127**, (1982).
- 777 44. Freeman, J. *et al.* Mapping brain activity at scale with cluster computing. *Nat. Methods*  
778 **11**, 941–950 (2014).
- 779 45. Migault, G. *et al.* Whole-Brain Calcium Imaging during Physiological Vestibular

780 Stimulation in Larval Zebrafish Article Whole-Brain Calcium Imaging during  
781 Physiological Vestibular Stimulation in Larval Zebrafish. *Curr. Biol.* **28**, 3723–3735  
782 (2018).

783 46. Ronzitti, E. *et al.* Recent advances in patterned photostimulation for optogenetics.  
784 *Journal of Optics (United Kingdom)* **19**, 113001 (2017).

785 47. Accanto, N. *et al.* Multiplexed temporally focused light shaping for high-resolution  
786 multi-cell targeting. (2018). doi:10.1364/OPTICA.5.001478

787 48. Shemesh, O. A. *et al.* Temporally precise single-cell-resolution optogenetics. *Nat.*  
788 *Neurosci.* **20**, 1796–1806 (2017).

789

## 790 **Acknowledgements**

791 We would like to thank Mykola Kadobianskyi for providing us with an early access to the  
792 *Danioella translucida* genome. Thanks to Adrien Jouary and Michael Orger for sharing their  
793 expertise in animal tracking and Roshan Jain for helpful discussion. G.R. was supported by a  
794 European Union's Horizon 2020 research and innovation programme under the Marie  
795 Skłodowska-Curie grant agreement No 666003, a Fondation pour le Recherche Medicale  
796 (FRM) 4th year doctoral fellowship and a Sorbonne University Postdoctoral Fellowship. Work  
797 in the laboratory of F.D.B. was supported by ANR-18-CE16 "iReelAx", UNADEV in  
798 partnership with ITMO NNP/AVIESAN (national alliance for life sciences and health), the  
799 Fondation Simone and Cino del Duca the Programme Investissements d'Avenir IHU  
800 FOReSIGHT (ANR-18-IAHU-01). B.J. acknowledges support by the German Research  
801 Foundation (DFG, project EXC-2049-390688087 and project 432195732), the Einstein  
802 Foundation (EPP-2017-413), the European Research Council (ERC- 2016-StG-714560) and  
803 the Alfried Krupp Foundation. C.G. was supported by an EMBO Short-term Fellowship, an

804 Institut Curie Postdoctoral Fellowship and an FRM Postdoctoral Fellowship. G.D. was  
805 supported by H2020 European Research Council (71598).

806

### 807 **Author Contributions**

808 G.R. and F.D.B. conceived the project with inputs from C.W., G.D. and C.G. G.R. designed all  
809 the experiments, developed the behavior rig and transgenic fish, and performed all the  
810 experiments and analysis unless otherwise specified. J.L. performed the analysis of the whole-  
811 brain data with inputs from G.R. under the supervision of G.D. M.C.T. and G.R. performed the  
812 backfill experiments under the supervision of C.W. K.D. and G.R. performed the other  
813 anatomical experiments. D.T. and G.F. performed the optogenetic experiment and analysis  
814 under the supervision of V.E. T.P. and R.C. built the light-sheet imaging rig. J.H., B.J. and  
815 R.B. obtained data from the field study. F.D.B. and C.G. supervised G.R. G.D. wrote the  
816 MSD/reorientation analysis script. The manuscript was written by G.R. and F.D.B. with inputs  
817 from other authors. All authors read and approved the final manuscript.

818